

Supplementary Information

Novel thiophene-based donor-acceptor scaffolds as cathodes for rechargeable aqueous zinc-ion hybrid supercapacitor

Haijun Peng,^[a] Yongxiang Zheng,^[b] Cyril Antheaume,^[a] Paolo Samorì ^{*[a]} and Artur Ciesielski ^{*[a]}

^a University of Strasbourg, CNRS, ISIS UMR 7006, 8 Allée Gaspard Monge, F-67000 Strasbourg (France). E-mail: ciesielski@unistra.fr , samori@unistra.fr

^b University of Strasbourg, Membrane Biophysics and NMR, Institute of Chemistry, UMR 7177, 1 Rue Blaise Pascal, F-67000 Strasbourg (France)

Table of Contents

Section A. Materials and Characterization	S2
Section B. Physical Characterization	S3
Section C. Electrochemical Measurements	S5
Section D. References	S7

Section A. Materials and Characterization

1) Materials

All commercially available reagents and solvents were purchased from Sigma Aldrich and used as received without further purification. Zinc foil (thickness of 100 μm), steel gauze (SSG), and coin cells obtained from Alfa Aesar and Pred Materials, respectively. Nonwoven separator MPF30AC (Japan, NKK), 2,5-Thiophene dicarboxaldehyde (TDA) and [2,2'-Bithiophene]-5,5'-dicarboxaldehyde (BTDA) was purchased from TCI, 2,2',2''-(benzene-1,3,5-triyl)triacetonitrile (BTAN) was prepared according to the previously reported procedure.¹

2) Characterization

The structure, composition and texture properties of materials were investigated by X-ray powder diffraction (XRD) with a Bruker D8 X-ray diffractometer, and Fourier transform infrared (FT-IR) with a JASCO, FT-IR 4700 Fourier Transform Infrared Spectrometer equipped with ATR Diamond. Thermogravimetric analyses (TGA) decomposition curves are recorded in the range 25-800 °C operating under nitrogen atmosphere, with a thermal step of 10 °C/min on a Mettler Toledo TGA/SDTA851e system. The specific surface area was measured using a Micromeritics ASAP 2050 surface area and porosity analyzer. Prior to the BET measurements, the samples were outgassed for 10 hours at 100 °C. Adsorption isotherms were calculated for nitrogen adsorption at 77 K and pressures up to 1 bar. Scanning Electron Microscopy (SEM) images were recorded with a FEI Quanta FEG 250 instrument S3 (FEI corporate, Hillsboro, Oregon, USA). Chemical composition was assessed by X-ray Photoelectron Spectroscopy with a Thermo Scientific K-Alpha X-ray photoelectron spectrometer equipped with an aluminium X-ray source (energy 1.4866 keV) at a vacuum level of 10^{-8} - 10^{-9} mbar in the main chamber. The spot size of the X-ray beam was fixed at 400 μm . High resolution transmission electron microscopy (HR-TEM) was performed on a JEOL 2100 F microscope working at 200 kV, equipped with a Cs probe corrector and a GATAN Tridiem imaging filter. The samples were prepared by applying a drop of dispersion containing graphene flakes on a TEM grid covered by a lacey carbon membrane. The as-prepared grids were kept overnight under high vacuum in order to remove the eventual solvent residues and possible contaminants. UHPLC: ThermoFisher Ultimate3000 with Scientific Vanquish Flex UHPLC, Detector : Vanquish PDA (VF-XX), followed by High Resolution Mass Spectrometry ThermoFisher Orbitrap : Exactive Plus with Extend Mass Range: Source HESI II. Column Reverse Phase : Thermo Fisher C18 Hypersil GOLD, 2.1 mm \times 100 mm, 1.9 μm , \leq 5 ppm.

Both, 1D and 2D-NMR spectra were recorded on a Bruker Ascend-500 Magnet, equipped with a Bruker Prodigy CryoProbe, using a Bruker AVANCE Neo as electronic bay. ^1H NMR are reported in ppm using solvent as internal standard for proton referencing (500 MHz, residual CHCl_3 at 7.26 ppm). $^{13}\text{C}\{^1\text{H}\}$ NMR spectra were also reported in ppm using solvent as internal standard (125 MHz, CDCl_3 at 77.3 ppm).

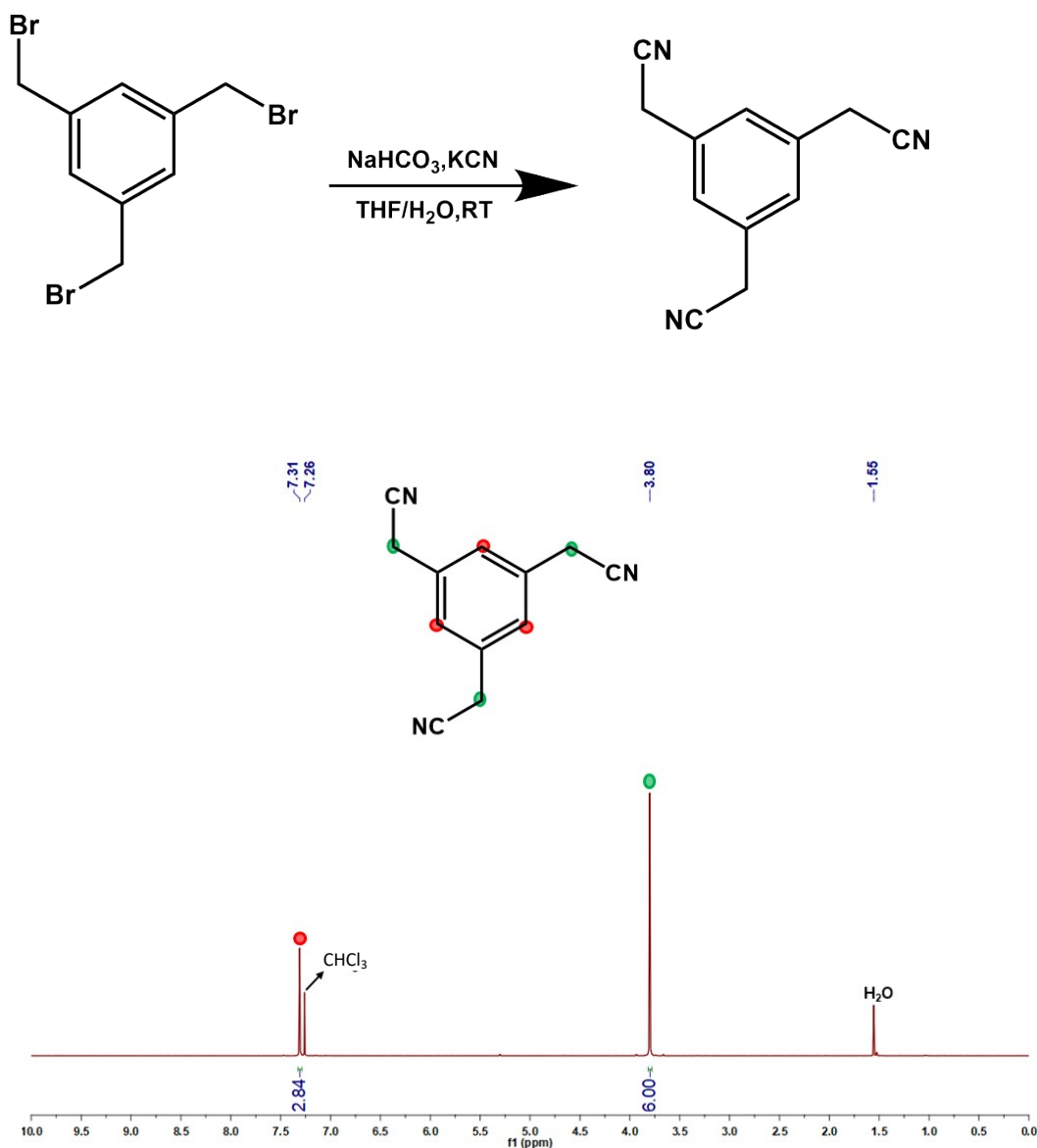
Fabrication of Zn-HSC

Zinc foil was directly used as anode electrode after polished with gauze and pouched into electrodes with 12 mm diameter. The cathode electrode composes of 60 wt% of TDA-1 or -2, 30 wt % of Super P conductive additives and 10 wt% of polyvinylidene fluoride as binder, 1-methyl-2-pyrrolidone was used as a dispersing agent. The mixed slurry was smeared on a porous stainless steel current collector and dried in a vacuum oven at 80 °C overnight (mass loading of active materials on stainless steel between 0.7 and 1.2 mg cm^{-2}). Zinc-ion hybrid supercapacitors were assembled with electrolyte of 2 M $\text{Zn}(\text{CF}_3\text{SO}_3)_2$ aqueous solution, Nonwoven separator MPF30AC as separator and coin battery shell.

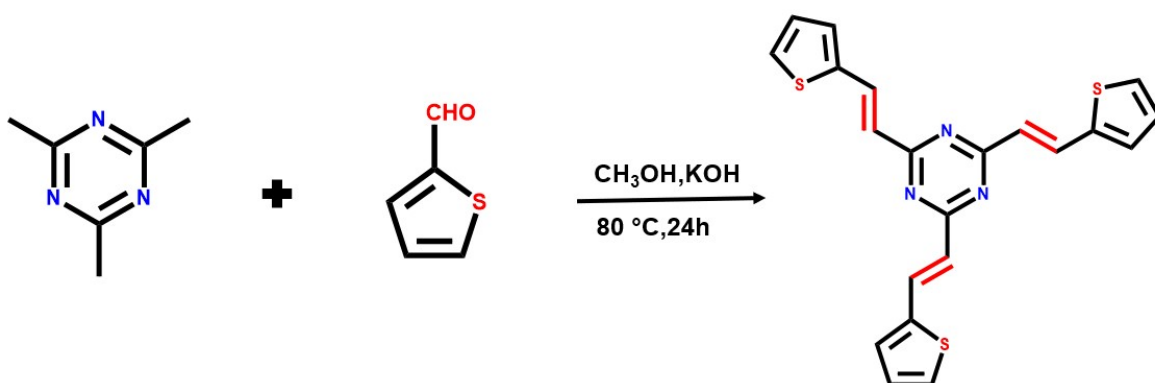
Electrochemical characterizations and calculations of Zn-HSC

Electrochemical performance of Zn-HSC was studied using cyclic voltammetry (CV), electrochemical impedance spectroscopy (EIS) on Autolab PGSTAT128N Potentiostat / Galvanostat instruments with a Metrohm Autolab DuoCoin Cell Holder (Metrohm AG) at room temperature. CV was performed at scan rates of 10 - 200 mV s^{-1} in the voltage range between 0 and 1.6 V. EIS measurement was measured with a frequency range of 0.01 Hz to 1 MHz.

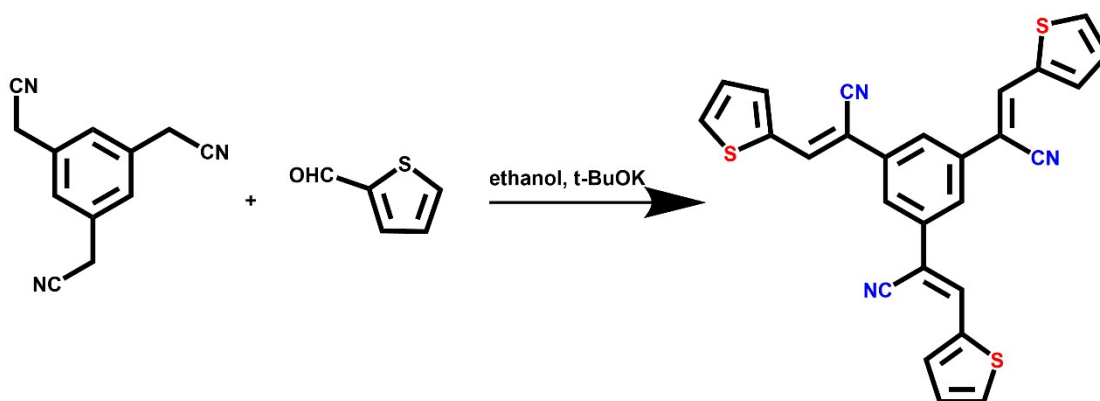
Synthesis of 1,3,5-Benzenetriacetonitrile (BTAN) Prepared as previous reported literature,¹ to a solution of 1,3,5-tris(bromomethyl)benzene (3.02 g, 8.50 mmol) in THF (25 mL) was added sodium bicarbonate (saturated solution, 30 mL) and sodium cyanide (4.17 g, 85.0 mmol) followed by 30 mL water. The solution was left to stir for 3 days after which it was acidified with 1 M HCl. THF was removed via rotary evaporation to leave behind 1.46 g (88%) of an off-white solid. ¹H NMR (CDCl₃, δ(ppm)): 7.31 (s, 3 H), 3.80 (s, 6 H), IR: ν 2239 cm⁻¹ (C≡N).



Synthesis of TDA-1: In a typical experiment, 2-thiophenecarboxaldehyde (5 mmol) was added to 2,4,6-trimethyl-1,3,5-triazine (5.7 mmol) in 70 ml of ethanol followed by the addition of 0.35 mmol of potassium tert-butoxide (t-BuOK). A light-yellow precipitate separates immediately, but the solution was stirred for another hour. Finally, the precipitate was filtered and washed with ethanol and was dried giving a yellow solid (yield 80%).



Synthesis of TDA-2: In a typical experiment, 2-thiophenecarboxaldehyde (5 mmol) was added to BTAN (5.7 mmol) in 70 ml of ethanol followed by the addition of 0.35 mmol of potassium tert-butoxide (t-BuOK). A yellow precipitate separates immediately, but the solution was stirred for another hour. Finally, the precipitate was filtered, washed with ethanol and was dried giving a yellow solid (yield 80%).



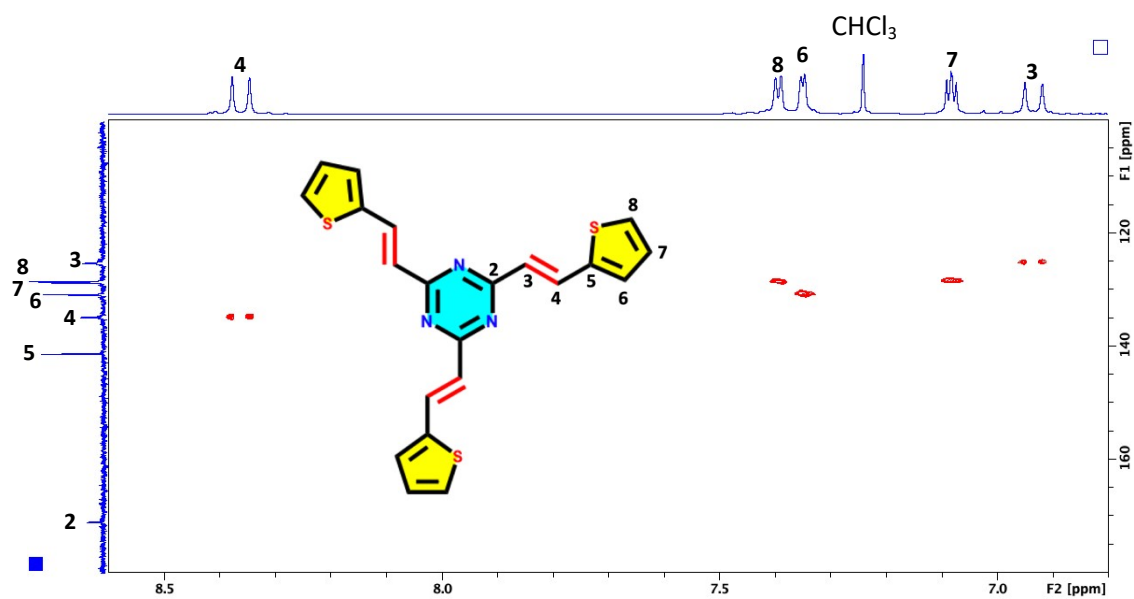


Figure S1. 2D ^1H - ^{13}C HSQC NMR spectra of TDA-1

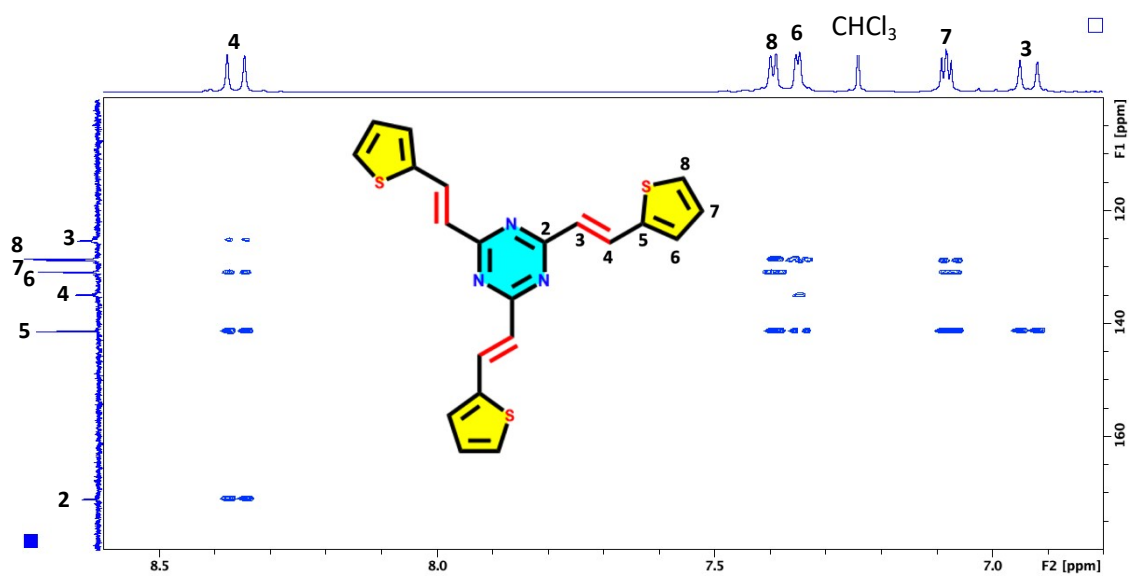


Figure S2. 2D ^1H - ^{13}C NMR spectra of HMBC for TDA-1.

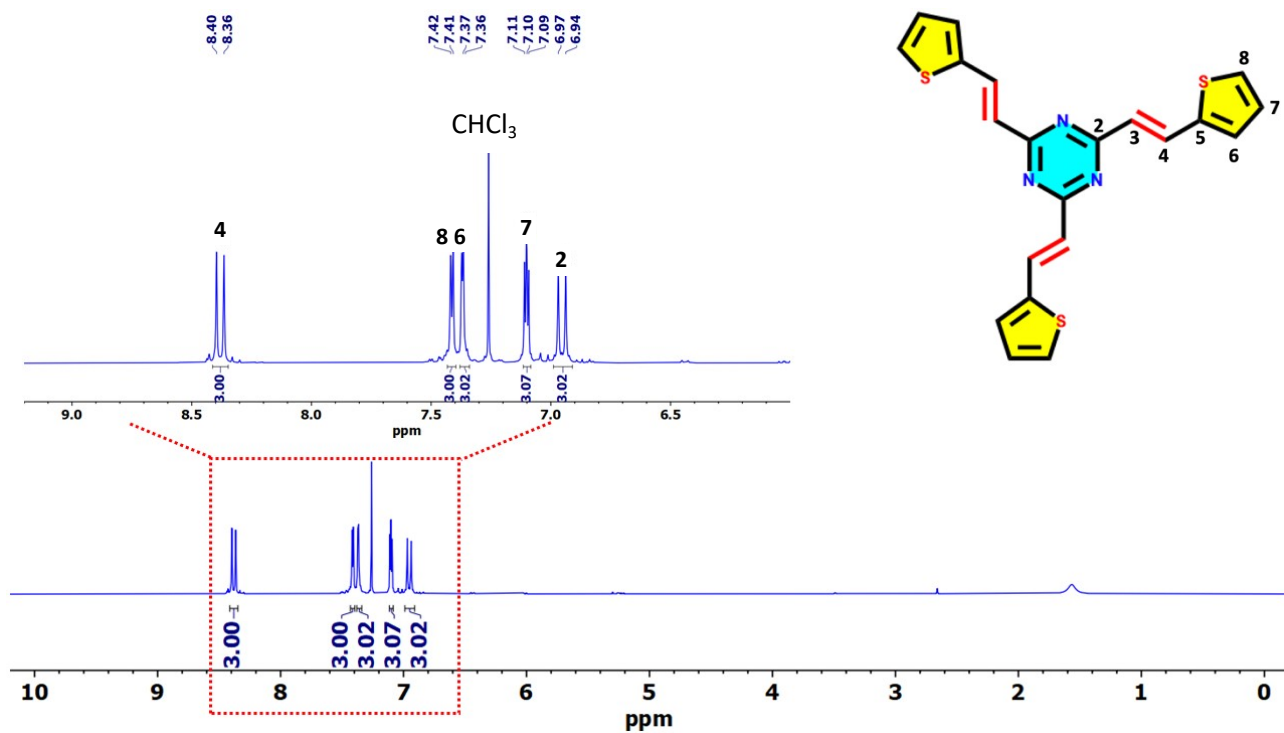


Figure S3. 1D ^1H NMR spectra for TDA-1.

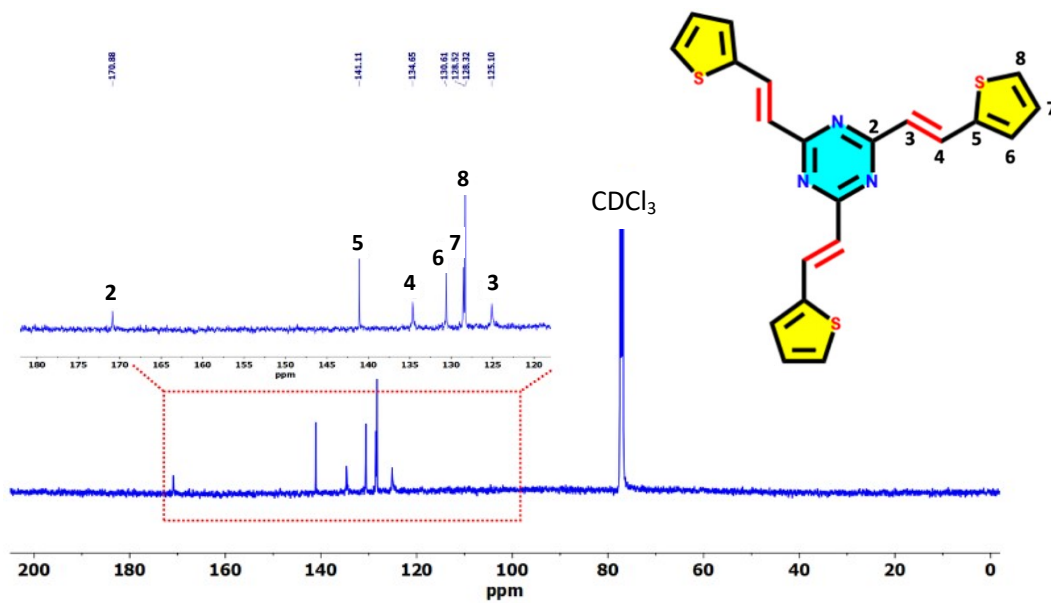


Figure S4. ^{13}C NMR resonance spectra of TDA-1

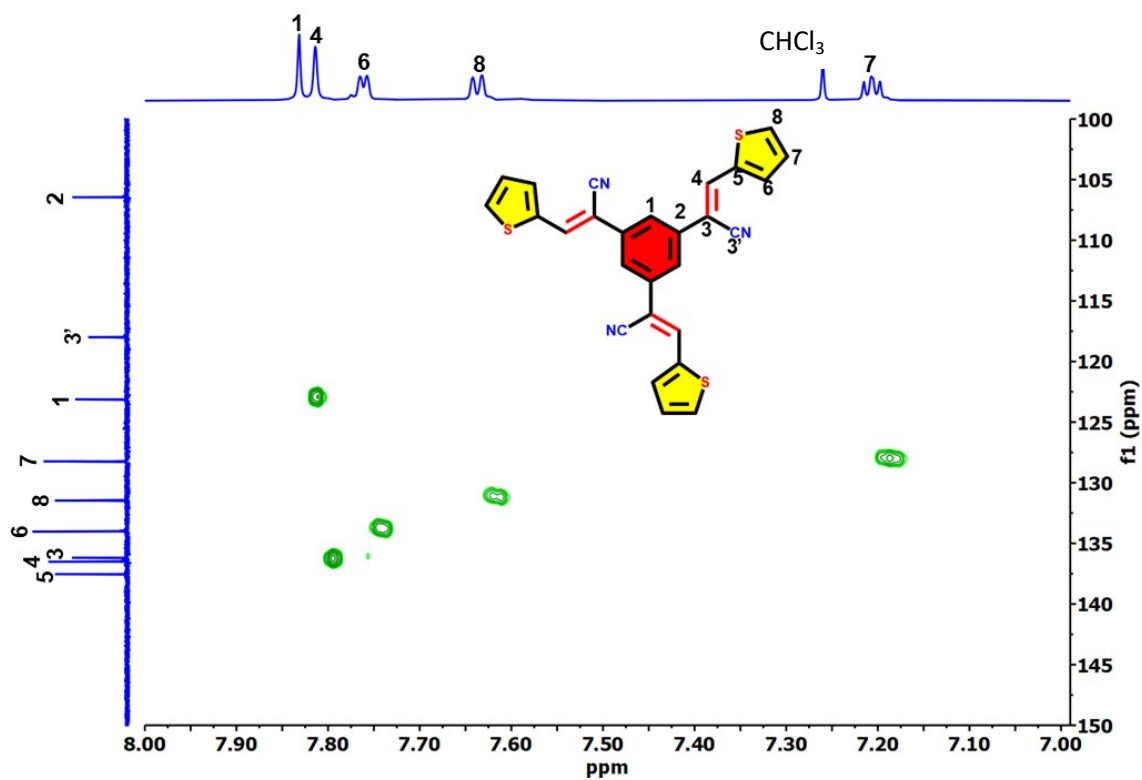


Figure S5. 2D ^1H - ^{13}C NMR spectra of HSQC for TDA-2

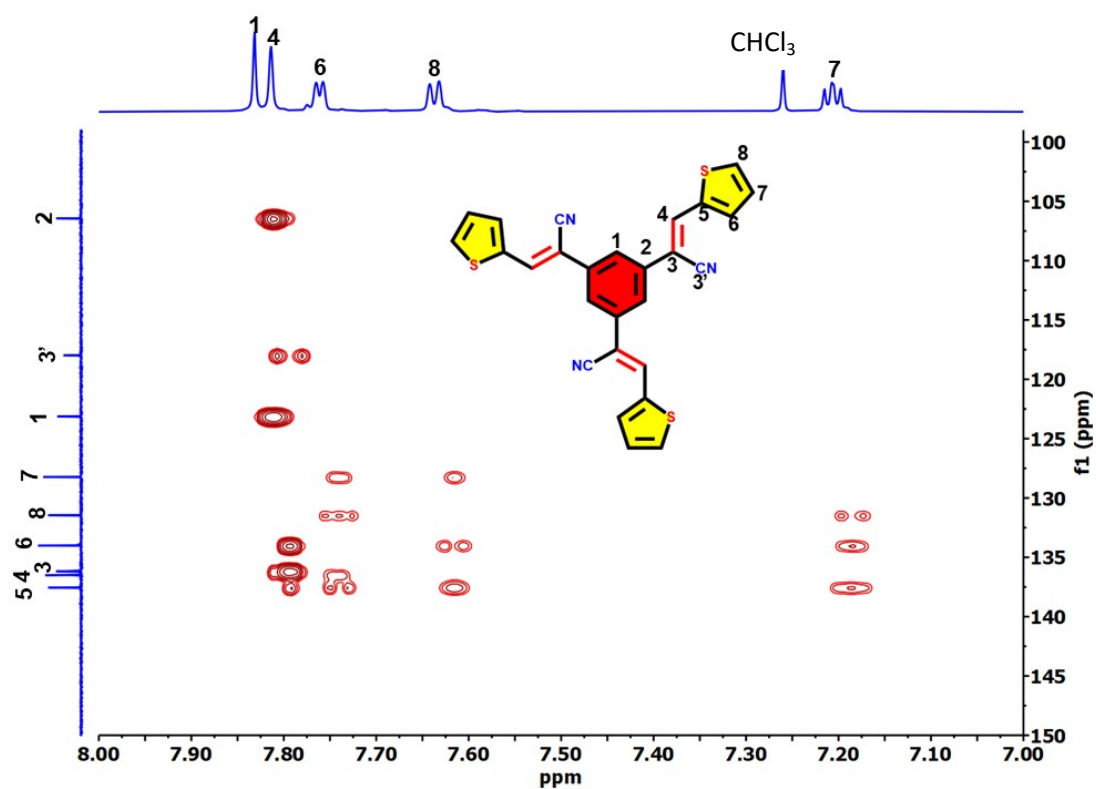


Figure S6. 2D ^1H - ^{13}C NMR spectra of HMBC for TDA-2.

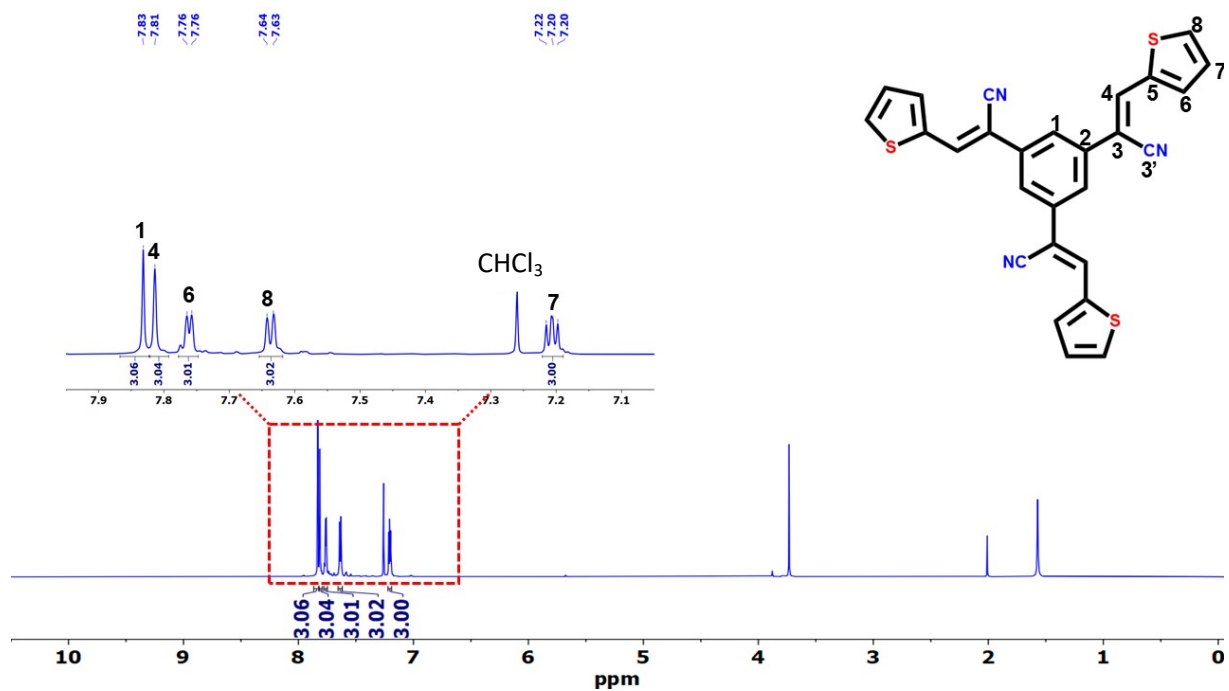


Figure S7. 1D ¹H NMR spectra for TDA-2.

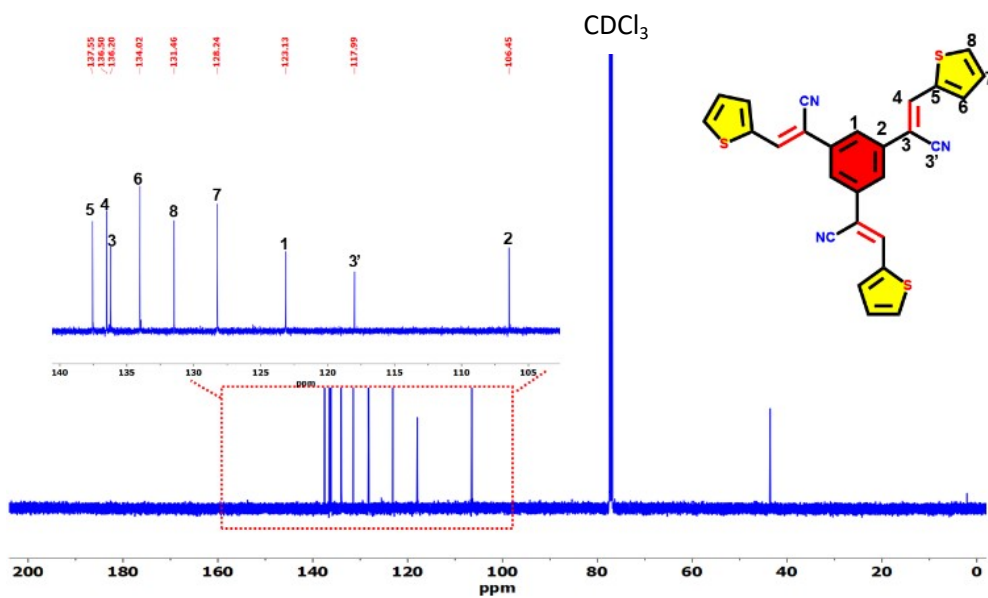
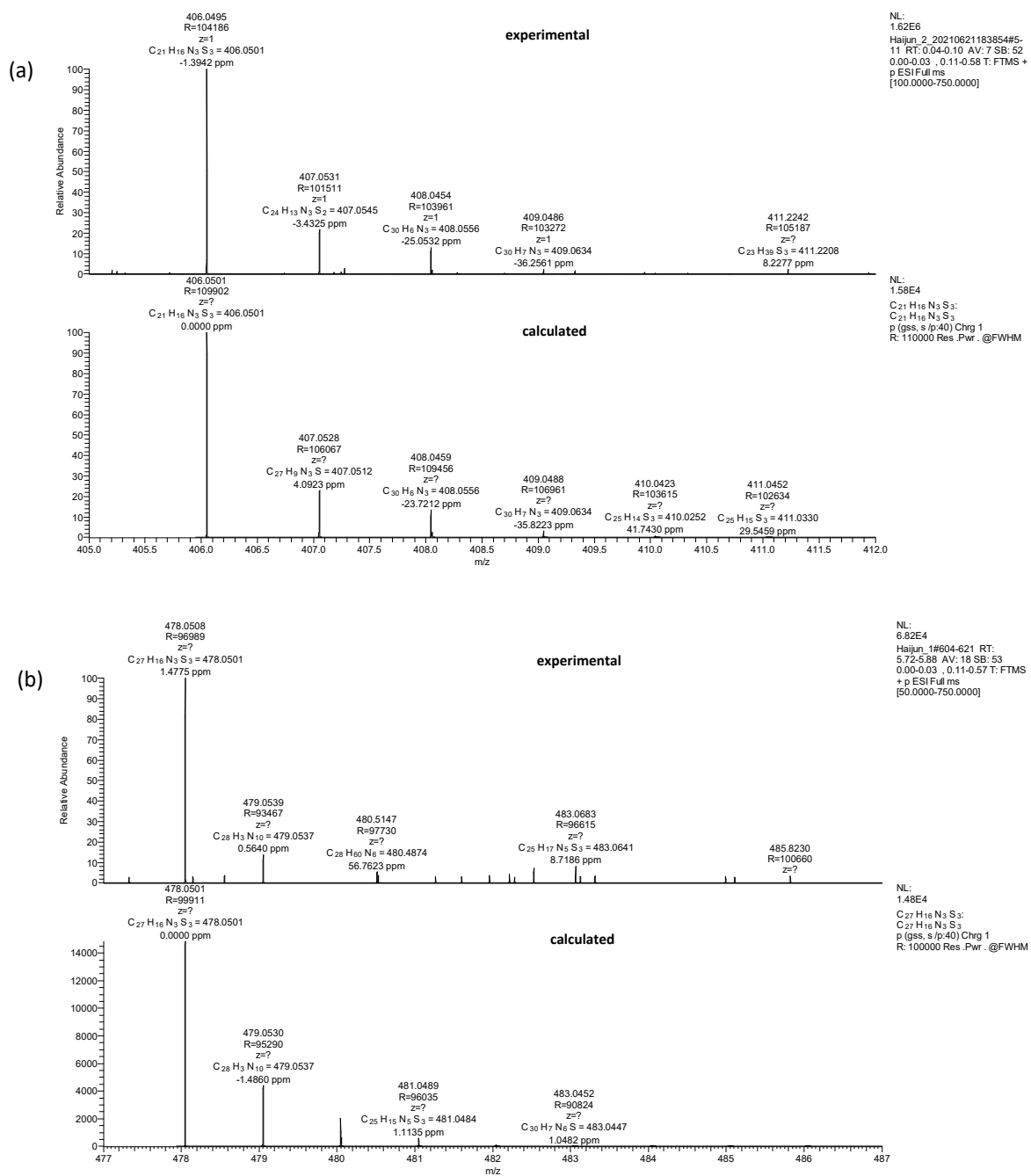


Figure S8. ¹³C NMR resonance spectra of TDA-2



TDA	-1			-2		
Peak	$\delta^{13}\text{C}$ [ppm]	$\delta^1\text{H}$ [ppm]	m, J (Hz)	$\delta^{13}\text{C}$ [ppm]	$\delta^1\text{H}$ [ppm]	m, J (Hz)
1				123.0	7.81	s
2	171.0	-		106.3	-	
3	125.1	6.93	d, 15.51 (E)	136.0	-	
3'				117.8	-	
4	134.7	8.31	d, 15.51 (E)	136.3	7.79	s
5	141.2	-		137.4	-	
6	130.6	7.34	d, 3.44	133.9	7.74	d, 4
7	128.4	7.08	dd	128.1	7.18	dd
8	128.6	7.39	d, 4.94	131.3	7.62	d, 5
$\text{CDCl}_3/\text{CHCl}_3$	77.3	7.26		77.3	7.26	

Table S1. ^1H NMR (δH in ppm, 500 MHz) and ^{13}C NMR (δC , 125 MHz) spectroscopic data of TDA-1 and -2 (both in CDCl_3)

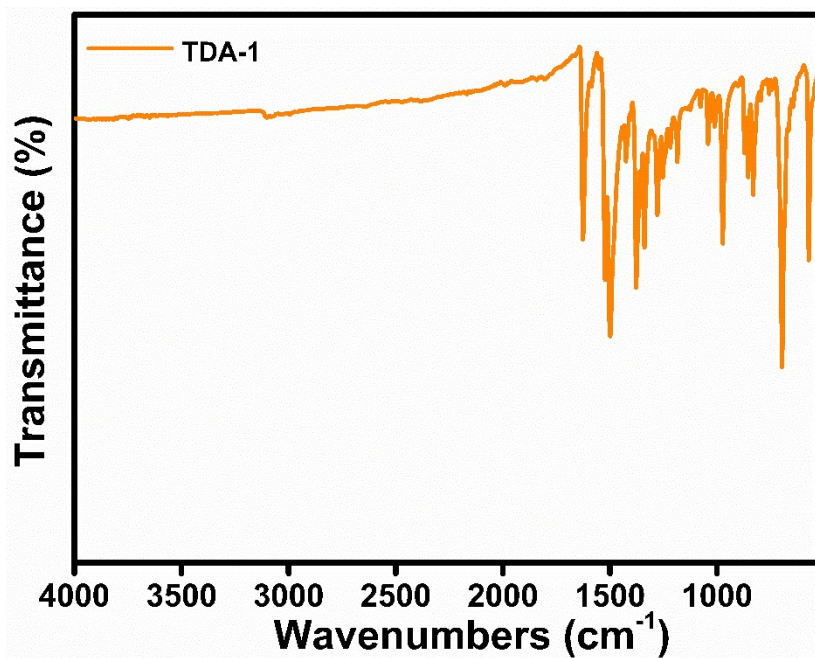


Figure S10. FT-IR spectra for TDA-1.

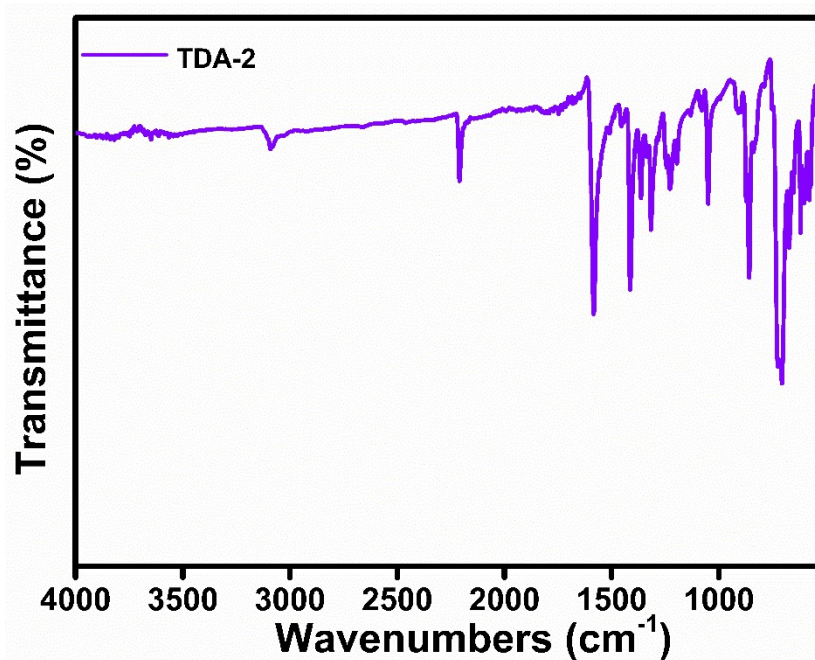


Figure S11. FT-IR spectra for TDA-2.

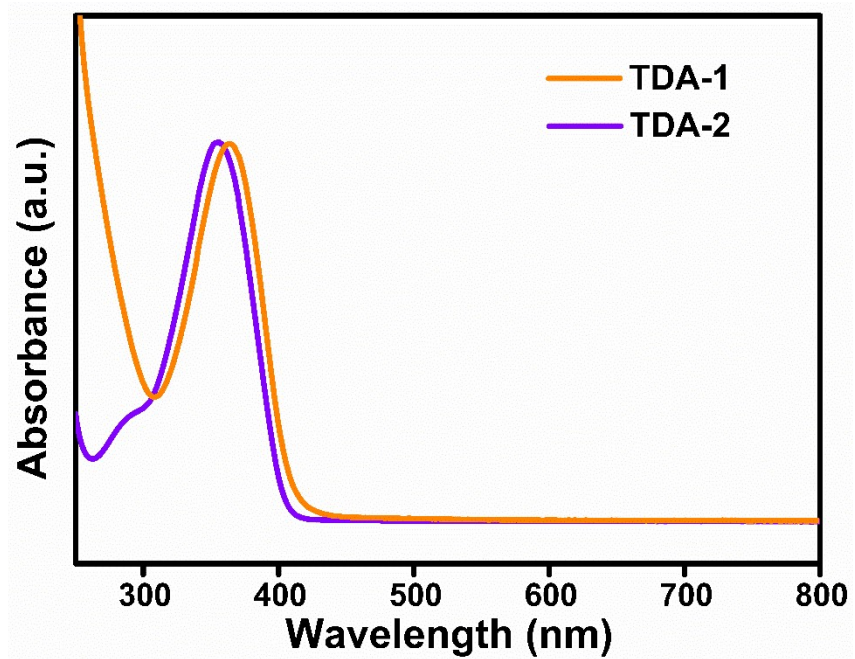


Figure S12. UV-Vis spectra for TDA-1 and -2.

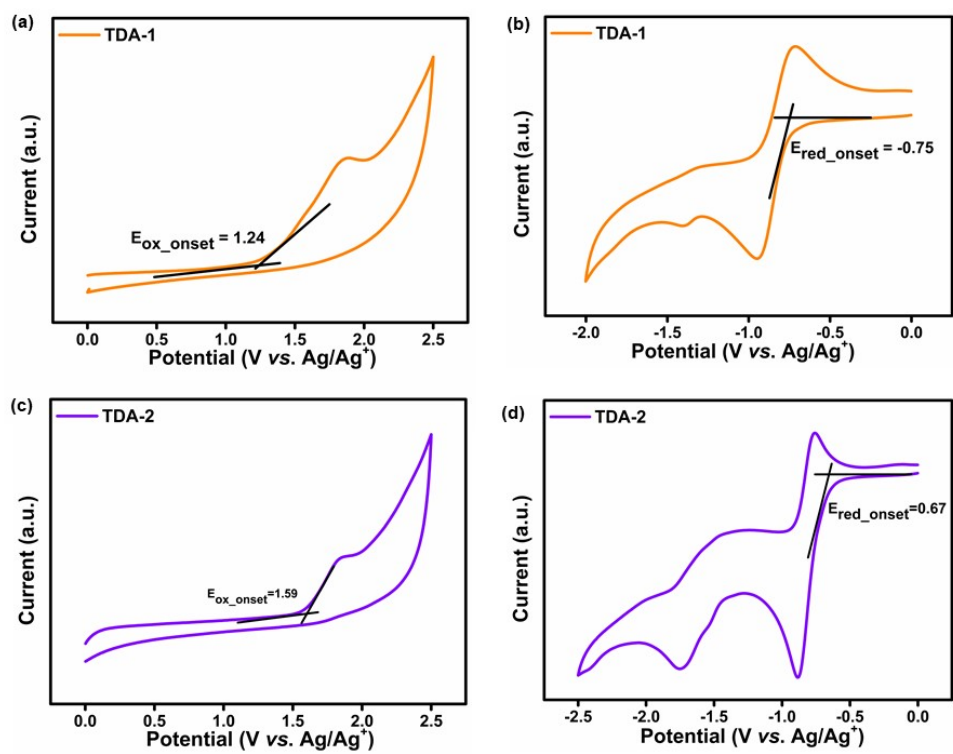


Figure S13. Cyclic voltammetry measurements of TDA-1(a) and (b), TDA-2 (c) and (d).

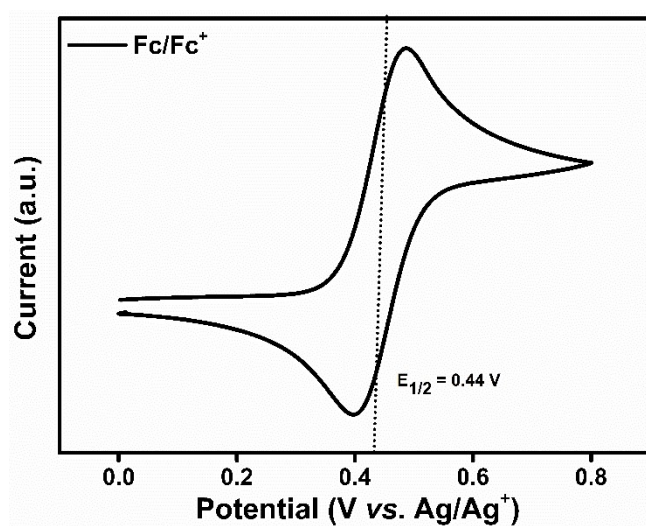


Figure S14. Cyclic voltammetry measurements of ferrocene/ferrocenium couple to calibrate the pseudo reference electrode.

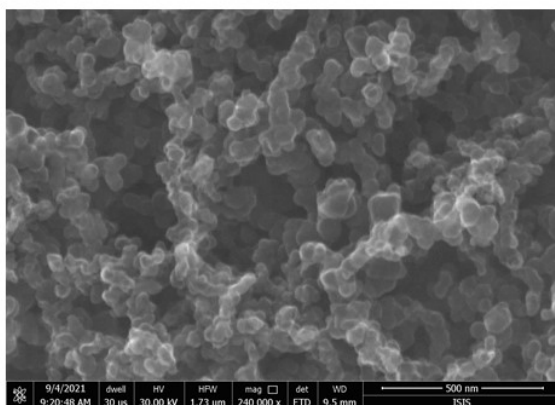
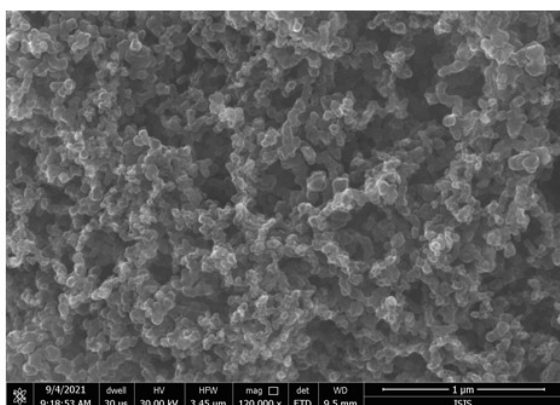
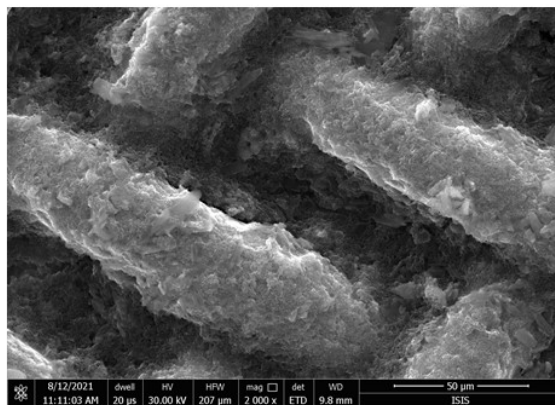
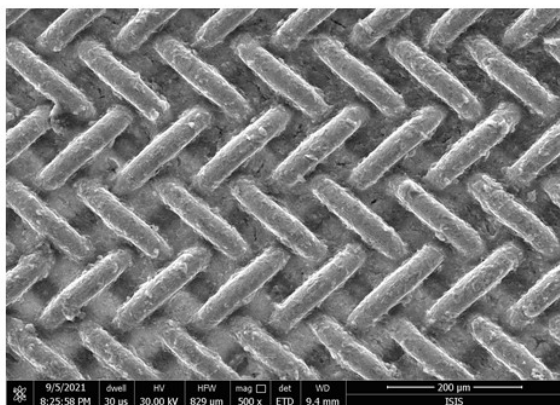


Figure S15. SEM images of TDA-1 electrode.

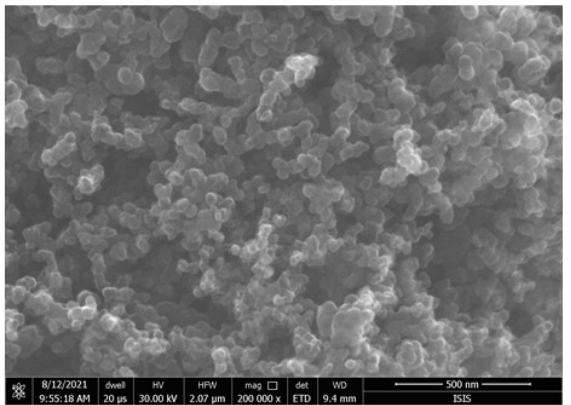
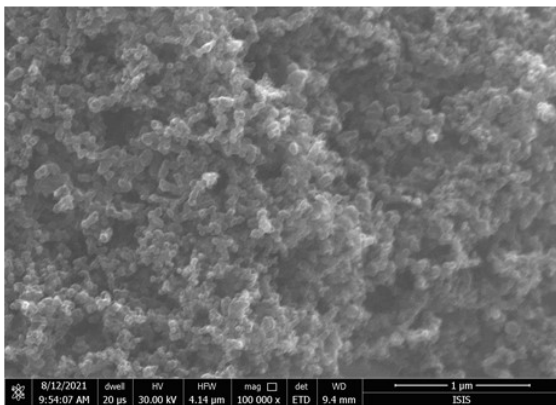
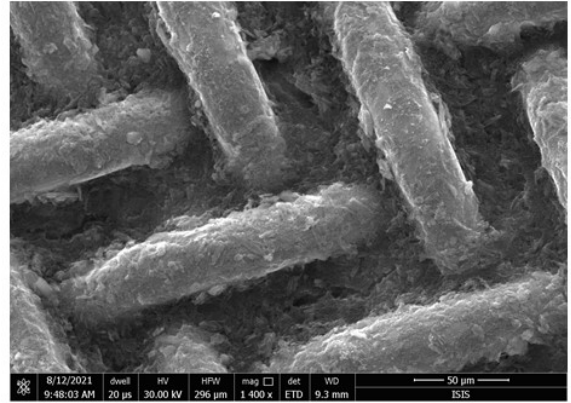
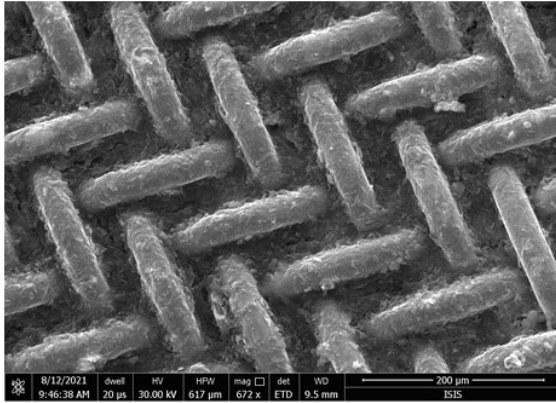


Figure S16. SEM images of TDA-2 electrode.

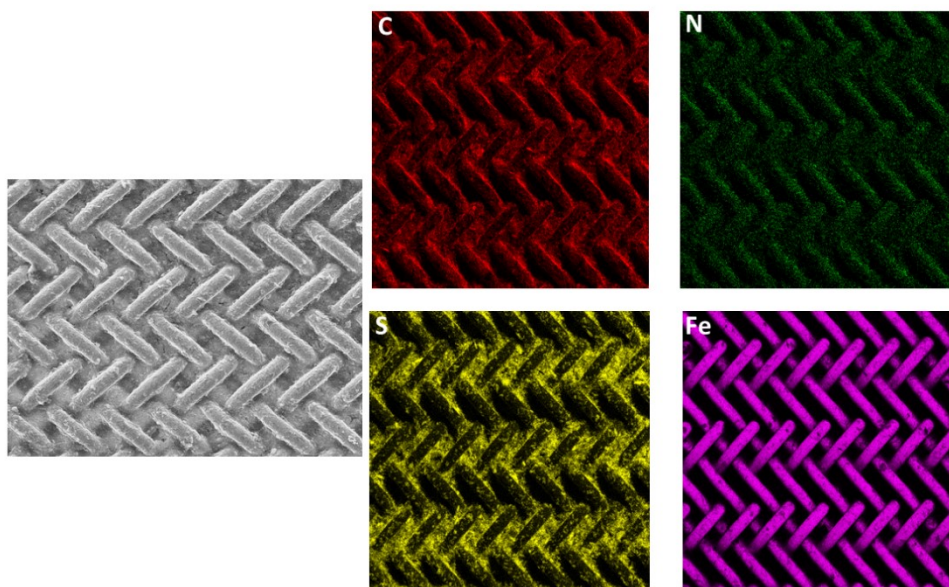


Figure S17. EDS spectra of C, N, S elements for TDA-2 on the stainless-steel current collector (Fe).

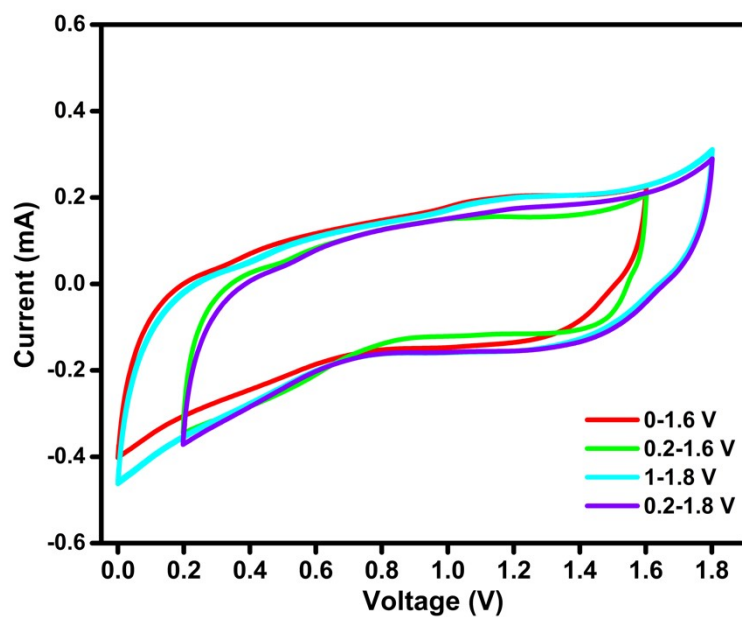


Figure S18. CV curves of pure Super-p electrode in Zn-HSC devices.

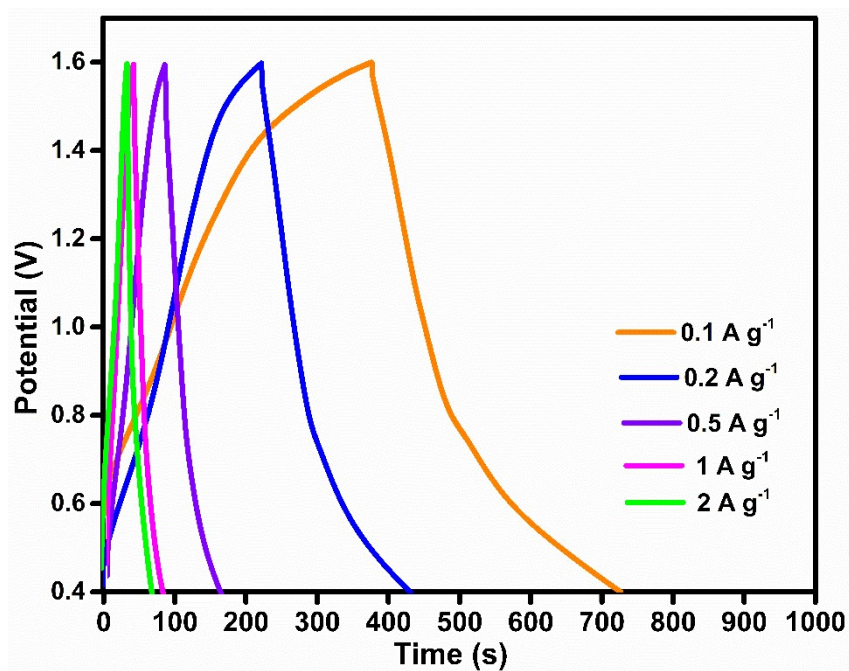


Figure S19. The galvanostatic charge/discharge curves of TDA-1 electrode at various current densities.

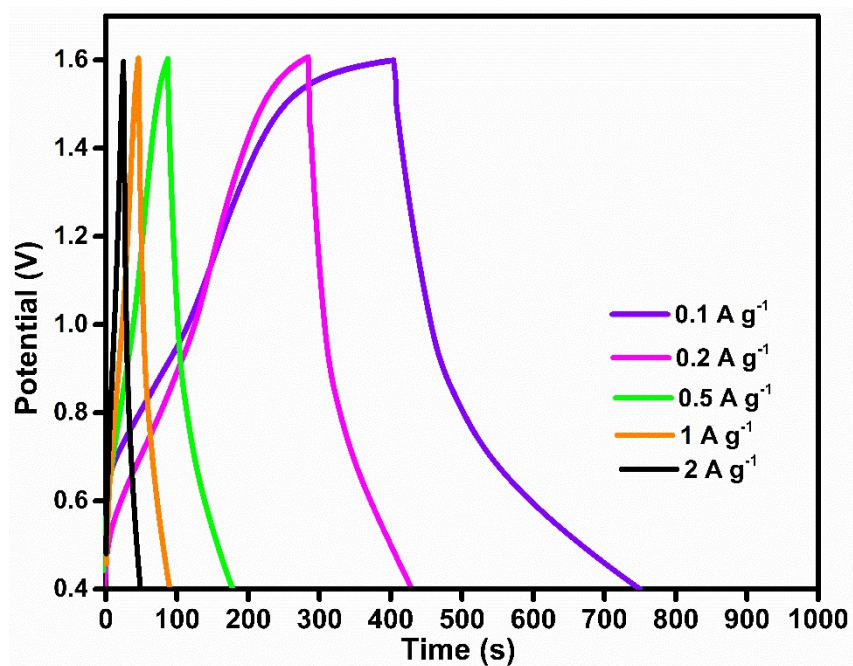


Figure S20. The galvanostatic charge/discharge curves of TDA-2 electrode at various current densities.

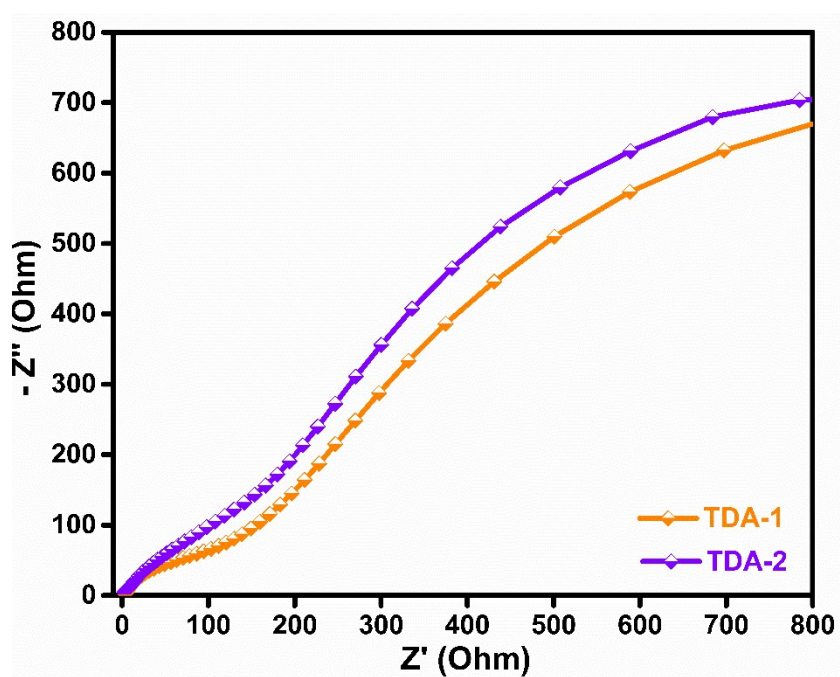


Figure S21. Nyquist electrochemical impedance spectra of TDA-1 and -2 cathodes.

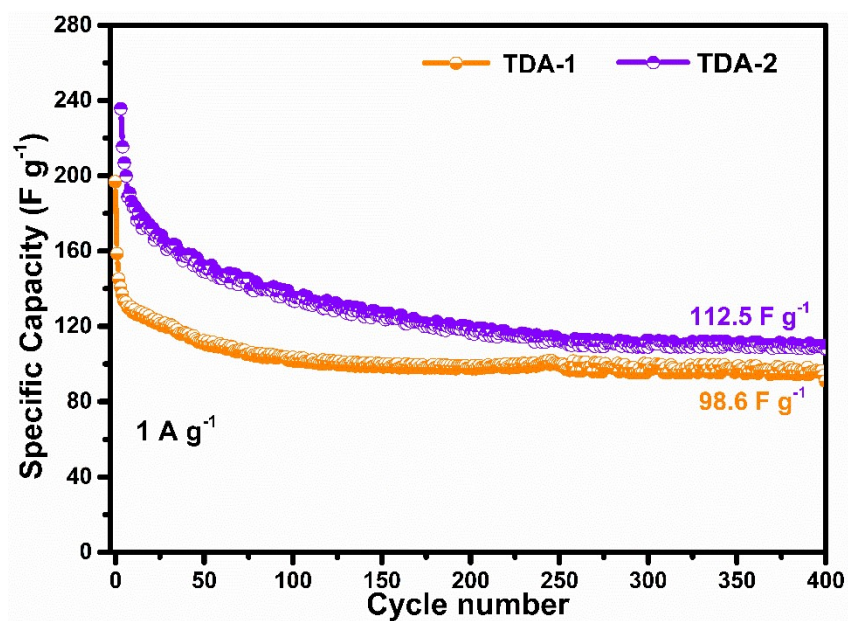


Figure S22. Cycle performance of TDA-1 and -2 electrodes at a current density of 1 A g⁻¹

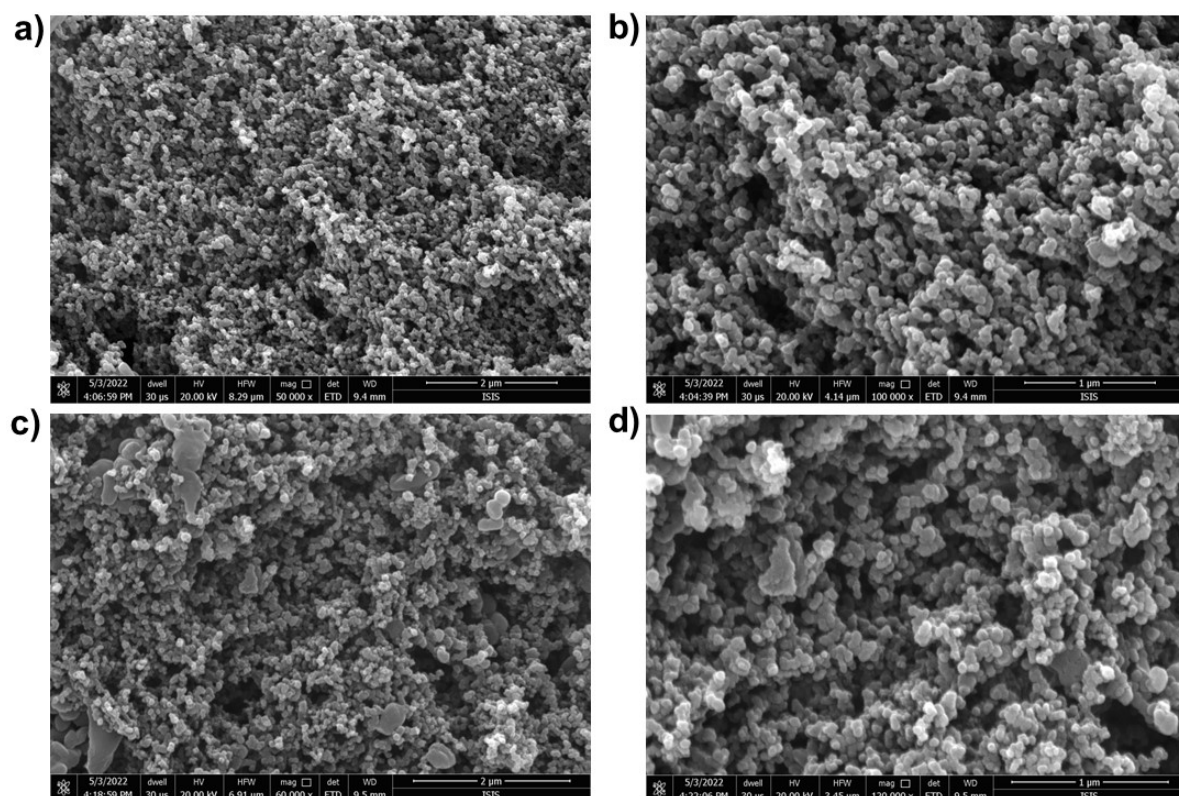


Figure S23. SEM images of Zn-HSCs device after 400 cycles for a-b) TDA-1, c-d) TDA-2 electrode.

Table S2. Capacitance comparison of our TDA-1 and TDA-2 electrodes compared to recently reported inorganic and organic compounds cathode materials for aqueous Zn-HSCs.

Material type	Electrode	Electrolyte	Voltage (V)	Current density / A g ⁻¹	Capacity / F g ⁻¹	Ref
Inorganic compounds	PDA@3DVAG	2M ZnSO ₄	-0.8-0.8	0.5	96.7	[2]
				2	59.8	
	Bio-carbon	1M Zn(CF ₃ SO ₃) ₂	0-1.8	0.1	170	[3]
				1	144	
	Zn-Ti ₃ C ₂ MXene	1M ZnSO ₄	0.1-1.4	0.5	132	[4]
				3	118	
	3D Mxene@rGo	2M ZnSO ₄	0.2-1.6	0.4	128.6	[5]
				6	40.3	
	Porous carbon	2M ZnSO ₄	0.-1.8	0.68	136.5	[6]
				10.88	72.9	
Organic compounds	Porphyrin polymer	2M ZnSO ₄	0.1-1.5	0.13	172	[7]
				1.5	94	
	Tetrachloro-1,4 benzoquinone	1 M Zn(CF ₃ SO ₃) ₂	0.8-1.4	0.217	118	[8]
	PQ-D	3M Zn(CF ₃ SO ₃) ₂	0.25-1.6	0.03	225	[9]
				0.15	210	
	DTT	2M ZnSO ₄	0.3-1.4	0.2	175	[10]
				2	99	
	Phenothiazine	2M ZnSO ₄	0.5-1.7	0.04	188.24	[11]
				0.1	145.56	
	PI-COF	2M ZnSO ₄	-0.9-0	0.7	332	[12]
	PA-COF	1M ZnSO ₄	0.2-1.6	0.1	247	[13]
				5	93	
	TDA-1	2M Zn(CF₃SO₃)₂	0-1.6	0.1	206.7	This work
1				98.6		
TDA-2	2M Zn(CF₃SO₃)₂	0-1.6	0.1	235.2		
			1	112.5		

Reference:

1. A. Yassin, M. Trunk, F. Czerny, P. Fayon, A. Trewin, J. Schmidt, A. Thomas, *Advanced Functional Materials* **2017**, *27*, 1700233.
2. R. Cui, Z. Zhang, H. Zhang, Z. Tang, Y. Xue, G. Yang, *Nanomaterials* **2022**, *12*, 386.
3. H. Wang, M. Wang, Y. Tang, *Energy Storage Materials* **2018**, *13*, 1-7.
4. Q. Yang, Z. Huang, X. Li, Z. Liu, H. Li, G. Liang, D. Wang, Q. Huang, S. Zhang, S. Chen, C. Zhi, *ACS Nano* **2019**, *13*, 8275-8283.
5. Q. Wang, S. Wang, X. Guo, L. Ruan, N. Wei, Y. Ma, J. Li, M. Wang, W. Li, W. Zeng, *Advanced Electronic Materials* **2019**, *5*, 1900537.
6. S. Zeng, X. Shi, D. Zheng, C. Yao, F. Wang, W. Xu, X. Lu, *Materials Research Bulletin* **2021**, *135*, 111134.
7. F.-Z. Cui, Z. Liu, D.-L. Ma, L. Liu, T. Huang, P. Zhang, D. Tan, F. Wang, G.-F. Jiang, Y. Wu, *Chemical Engineering Journal* **2021**, *405*, 127038.
8. D. Kundu, P. Oberholzer, C. Glaros, A. Bouzid, E. Tervoort, A. Pasquarello, M. Niederberger, *Chemistry of Materials* **2018**, *30*, 3874
9. K. W. Nam, H. Kim, Y. Beldjoudi, T.-w. Kwon, D. J. Kim, J. F. Stoddart, *Journal of the American Chemical Society* **2020**, *142*, 2541.
10. Y. Wang, C. Wang, Z. Ni, Y. Gu, B. Wang, Z. Guo, Z. Wang, D. Bin, J. Ma, Y. Wang, *Advanced Materials* **2020**, *32*, 2000338.
11. N. Wang, Z. Guo, Z. Ni, J. Xu, X. Qiu, J. Ma, P. Wei, Y. Wang, *Angewandte Chemie International Edition* **2021**, *60*, 20826.
12. M. Yu, N. Chandrasekhar, R. K. M. Raghupathy, K. H. Ly, H. Zhang, E. Dmitrieva, C. Liang, X. Lu, T. D. Kühne, H. Mirhosseini, I. M. Weidinger, X. Feng, *Journal of the American Chemical Society* **2020**, *142*, 19570.
13. W. Wang, V. S. Kale, Z. Cao, S. Kandambeth, W. Zhang, J. Ming, P. T. Parvatkar, E. Abou-Hamad, O. Shekhah, L. Cavallo, M. Eddaoudi, H. N. Alshareef, *ACS Energy Letters* **2020**, *5*, 2256.